CO-LOCATED TRIANGULATION: SINGLE NODE DAMAGE POSITION IDENTIFICATION

Seth S. Kessler and Ajay Raghavan

Metis Design Corporation, Cambridge, MA USA

ABSTRACT

A fundamental limitation for current Structural Health Monitoring (SHM) systems is the need for distributed synchronous sensors to determine precise damage location using traditional triangulation methods. Accuracy is dictated by sensor density (quantity and proximity), which drives complexity, weight and cost to resolve reliable position. This paper introduces a patent-pending real-time method to predict accurate damage location from a single SHM node. This co-located triangulation method consists of novel sensors, algorithms and hardware to achieve a significantly more efficient means of localizing damage. Results are presented for proof-of-concept experiments on an aluminum plate using guided waves, as well as theoretical accuracy and limitations for the method. Finally, a description of a prototype under development is presented. SHM technology will be critical to reducing the overall cost of ownership for air and spacecraft, and the present research could play an important role in implementing such a system feasibly, practically and efficiently.

Index Terms— Structural Health Monitoring, Lamb Waves, damage detection, triangulation, piezoelectric sensor

1. INTRODUCTION

Structural Health Monitoring (SHM) implies the incorporation of a non-destructive evaluation system into a structure to provide continuous remote monitoring for damage. SHM has the overall goal of improving vehicle safety and reliability while reducing maintenance and inspection-based life-cycle costs. During the course of recent research, Lamb wave methods have been proven a reliable technique to collect valuable information about the state of damage within a structure. Several investigators have successfully used Lamb waves to determine the presence and location of damage within both metallic and composite specimens [1-5]. Typically, Lamb wave methods are implemented using a distribution of piezoelectric elements propagating ultrasonic elastic waves in a "pitch-catch" mode. This results in measures of delayed and attenuated signals along each possible actuator and sensor path, as well as occasional scattered reflections from damage sites. This data can then be used to reconstruct damage location by using traditional triangulation calculations. While this methodology has shown promise, accuracy is dependent on the sensor network density. To resolve small damage precisely, a large array of sensors in close proximity must be employed, which increases the system complexity, weight and cost with additional wires, acquisition channels and volume of data. This tradeoff has presented a major obstacle to deploying a practical large-scale SHM system [6].

To remedy this dilemma, the present investigators have developed a patent-pending method to predict accurate damage location from a single SHM node. This co-located triangulation method uses a novel sensor design along with an innovative algorithm to greatly reduce the sensor density required to localize damage. By increasing efficiency without sacrificing accuracy, this methodology provides a feasible path to deploy a Lamb wave-based SHM system in commercial applications.

2. THEORY

The co-located triangulation methodology draws much of its benefit from the fact that it is "pulse-echo" based rather than "pitch-catch." In "pulse-echo" mode, an excitation radiates from a source (omni-directional Lamb waves in the present case) and subsequent reflections are measured from the same location. In the literature, "pulse-echo" testing has been achieved using "self-sensing" circuits, which allow a single element to excite and sense simultaneously or in quick succession, as well as side-by-side sensor and actuator elements [7]. While both of these methods have merit, they present logistical and analytical challenges that limit their applicability to most implementations.

Therefore, the present investigators have invented the patented concept of co-located sensor and actuator elements for "pulse-echo" applications, where co-planar elements are positioned in close proximity to substantially surround each other (i.e. an actuator circumscribing a collection of sensors or the converse). These elements can be physically unique, or created virtually through selective plating or poling. The present research embodies this concept with an SHM node comprising of 4-sensor and 1-actuator elements fabricated in a deliberate pattern from a single piezoelectric wafer. Using this node, co-located triangulation predictions can be realized by using complementary algorithms.

2.1. Algorithm

The damage site is assumed to be a Lamb wave scatter point described by its radial and angular position (r and ϕ) in a polar coordinate system, with the origin at the center of the SHM node. The time at which the peak of the wave packet originates from the damage site is t_s and t_i (i = 1 to 4) is the time the peak of the wave packet arrives at each of sensor element positions at radius a The orientation of the sensors for this derivation is shown in **Figure 1**.

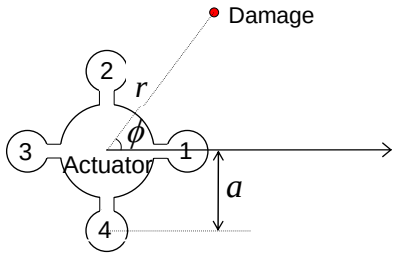

Figure 1: SHM node orientation and coordinate system

Distance to damage from each sensor can then be described by relating the group speed c_g and the respective times of flight:

$$(a - r\cos\phi)^2 + r^2\sin^2\phi = c_g^2(t_1^2 - t_s^2) \quad (1)$$

$$r^2\cos^2\phi + (a - r\sin\phi)^2 = c_g^2(t_2^2 - t_s^2) \quad (2)$$

$$(a + r\cos\phi)^2 + r^2\sin^2\phi = c_g^2(t_3^2 - t_s^2) \quad (3)$$

$$r^2\cos^2\phi + (a + r\sin\phi)^2 = c_g^2(t_4^2 - t_s^2) \quad (4)$$

Simplifying and consolidating equations 1-4 yields:

$$\tan\phi = \left(\frac{(t_4 - t_2).(t_4 + t_2 - 2t_s)}{(t_3 - t_1).(t_3 + t_1 - 2t_s)}\right) \quad (5)$$

Since the sensor pairs 1/3 and 2/4 are diagonally opposite and equidistant from the center, it is reasonable to assume that $(t_4 + t_2) \approx (t_3 + t_1)$. Therefore equation 5 can be simplified to:

$$\tan\phi = \left(\frac{t_4 - t_2}{t_3 - t_1}\right) \quad (6)$$

Solving for ϕ *yields the following pair of equations*:

$$\begin{aligned}\phi &= \text{atan2}(t_4 - t_2, t_3 - t_1) \ \text{ if } |t_4 - t_2| \geq |t_3 - t_1| \\ &= \text{atan2}(t_3 - t_1, t_2 - t_4) - \pi/2 \ \text{ otherwise}\end{aligned} \quad (7)$$

where atan2 is the four-quadrant inverse tangent function. In the experiments, sensor 1 was at 45° relative to the x-axis so results were offset by 45°. Finally, the radial distance was calculated based on the average time of flight from the four sensors:

$$r = 0.5c_g\left(\frac{t_1 + t_2 + t_3 + t_4}{4} - t_a\right) \quad (8)$$

where t_a is the peak of the excitation pulse.

Therefore, to solve for r and ϕ, each of these t values must be mined from the experimental data. Sensor response signals are detrended and filtered with zero-phase higher-order Butterworth filters to remove noise in the frequency bandwidth outside the excited range. The difference signal between the test and baseline signals are then produced, and convolved with the excitation signal to obtain the signal component at the central frequency. A Hilbert transform applied to this signal component produces a signal envelope, and a peak extraction algorithm applied to this envelope yields the times corresponding to the peaks of the reflections.

2.2. Method limitations

The accuracies of all wave-based methods rely on several parameters [7]. They parameters can be grouped into 3 interrelated categories: algorithm-dependant, specimen-dependant and hardware-dependant errors. While these sources of error can affect traditional wave-based methods, many of them have a more direct and significant impact on the presented method, however, due to the sensitivities of governing equations described above.

The most independent of these potential sources of error are the algorithm-dependant parameters. The algorithm must be robust towards poor signal-to-noise ratios as typically seen in wave propagation [7]. Next, the precision with which the reflection peaks can be identified by the algorithm is critical in determining corresponding time-of-flight. Without reliable peak detection, the precision of the algorithm rapidly deteriorates.

For specimen-dependant error, the first consideration is the ratio between size of the damage (d) and the wave mode wavelength (λ). If this ratio is too small, the damage causes weak reflection signals, leading to higher algorithm-based error. As this ratio approaches and exceeds unity, while the reflection are stronger, the "point source" assumption weakens. Consequently, sensors may detect reflections originating from different points of the damage site. Next, wave group speed c_g plays a straightforward role in location accuracy. It has a linearly proportional contribution with radial position calculation, as seen in equation (8), and the relative spacing between the peaks of the wave reflection from the damage site also decreases with increasing c_g, thereby increasing the potential for angular position calculated error.

The final consideration is hardware-dependant error. First, this is the main location for noise introduction, both from poor shielding and internal crosstalk. Care must be taken to guarantee good signal fidelity for the algorithm to be successful. The most fundamental limit, however, is placed on this method by the data sampling rate, which determines how precisely the individual peaks of reflections can be resolved. For example, in the present tests with a sampling rate of 10 MHz and a c_g of ~2.5 km/s, the angular error caused by an inaccuracy in peak determination by a single sample point is 1-2°. The corresponding error in radial location is negligible (~0.1 mm for damage at a radius of 25 cm). These errors are approximately inversely proportional to data sampling rate, and are linearly proportional to c_g.

3. VALIDATION

To validate this co-located triangulation methodology, prototype nodes and hardware were fabricated, and the algorithm was coded within Matlab™. The following sections describe the experimental procedure that was followed to localize representative damage in a large aluminum plate. While it was not possible to demonstrate every aspect of this methodology in this initial test, the results provide sufficient evidence to prove the concept valid.

3.1. SHM node design

A 4-sensor and 1-actuator element SHM node was fabricated to perform the prescribed tests. The node was shaped by laser from a single PZT-5A piezoelectric wafer, and selectively electrode and poled so that the 5 elements could be accessed independently with a common ground. A flexible circuit was designed to make electrical connections to appropriate electrodes and suppress EMI and cross-talk, while not impeding wave propagation. Subsequently, the wafer and flex-circuit were assembled using electrically conductive film-adhesive in an elevated temperature cure under vacuum, and a miniature multi-pin connector was installed to break out the signals to hardware, seen in **Figure 2**.

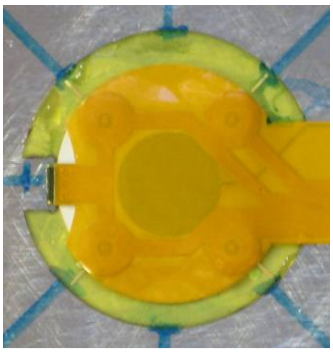

Figure 2: Photograph of prototype SHM node used for testing

3.2. Hardware design

To implement this method, 5 synchronously sampling channels of data acquisition were required (4 for the sensors and 1 for the actuator for precise timing) along with an arbitrary function generator and appropriate signal conditioning circuitry. A custom miniature 100 MHz hardware system was designed by the present investigators using their patented Point-of-Measurement™ technology, and a 5 x 10 x 20 cm prototype system was fabricated. While this prototype was able to successfully conduct testing and collect the required data, a design flaw led to a persistent overheating problem, requiring the system to re-boot frequently. Therefore in the interest of time, and since this hardware was not a critical element of the proof-of-concept, a 10 MHz Tektronix 3014B and Agilent 33220 units were used to collect the test data.

3.3. Experimental setup

The test specimen was a 0.9 meter square 3.2 mm thick 6061 aluminum plate. A circle of 0.5 meters in diameter was drawn centered on the plate, and ray lines were draw every 10° radiating from the origin. Thirty-six visual indicators were drawn at the intersections of the circle and the rays to mark the field of damage locations. A common "inverse damage" technique was used, where stiffness and mass is added to the specimen rather than removed so that representative damage could be introduced in a reversible, repositionable and reproducible fashion [8]. In this case, 3 sizes of small magnets (3.2, 6.4 and 12.7 mm diameter) were placed at the marked positions on the plate using shear couplant gel. Data was collected for each size magnet at each marked position.

3.4. Test parameters

The guided-wave (GW) mode wavelength and excitability curves were computed for the described configuration using previously developed models [9]. The fundamental antisymmetric (A_0) Lamb wave mode was strongest at 90 kHz, which was also well below the cutoff frequency for higher order modes. This mode was selected over the fundamental symmetric (S_0) mode since at this frequency it produces a seven times larger response, and the S_0 mode wavelength (5.94 cm) is much larger than the A_0 mode wavelength (1.67 cm) and the representative damage diameters. The actuation signal was a 3.5-cycle toneburst modulated by a Hanning window and therefore it can be considered to be narrowband excitation. All GW packets are assumed to travel at the A_0 mode group speed at 90 kHz (c_g= 2548 m/s). The baseline (undamaged) and test (damaged) signals were obtained by averaging 256 sensor response signals corresponding to periodic bursts to maximize the signal-to-noise ratio. There was a 300-ms delay between successive bursts to ensure that boundary reflections caused by one excitation burst did not interfere with the responses to the subsequent burst.

4. RESULTS

The experimental setup described in the previous section was executed using the specified test parameters. Data collection was PC automated, and the resulting voltage versus time files were streamed into a Matlab™ algorithm for processing. **Figure 3** presents the final algorithm results for predicted versus actual damage angular and radial position for each magnet size.

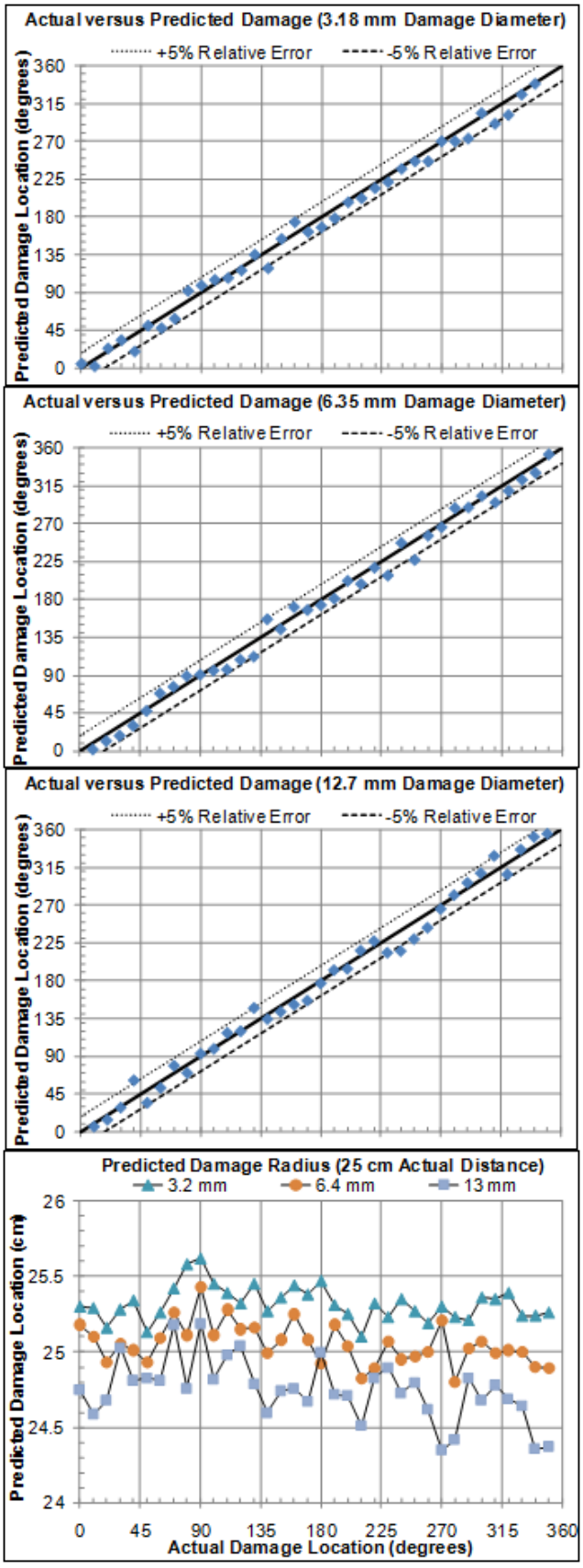

Figure 3: Experimental results for predicted angles and radii

5. DISCUSSION

The overall results from the algorithm exceeded expectations for a prototype system. While not quite achieving the theoretical accuracies for angle and radius position prediction, the average error values were quite low, and the maximum error values were still reasonable. Potential sources of error were described in a previous section, however since care was taken to minimize hardware-dependant error and the c_g for aluminum is simple to calculate, most of the error can be attributed to algorithm-dependant sources. A slight dependency on damage size was also observed, particularly for the angle prediction case.

5.1. Angular position

The results for angular position were presented in **Figure 3**. Here the data points represent the algorithm predictions for each of the 36 test points, the solid line represents the ideal case (prediction = actual) and the dashed lines represent ±5% error bounds (relative to 360°). A summary of the absolute value and percentage of maximum and average error can be seen in **Table 1**. Overall, the average error for all cases was 8.6° (2.4%), with the highest error falling at odd multiples of 45° and the lowest at multiples of 90°, as anticipated by inspecting equation (7). A slight dependency on damage size was observed, whereas the maximum error seems to increase slowly as the ratio of diameter to wavelength approaches unity (d/λ = 0.19, 0.38 and 0.76 respectively).

Table 1: Maximum and average angular position prediction error

Damage (mm)	*Max. Error (degrees)*	*Max. Error (%)*	*Avg. Error (degrees)*	*Avg. Error (%)*
3.18	21.1	5.9%	8.6	2.4%
6.35	22.9	6.4%	8.2	2.3%
12.7	24.3	6.8%	9.1	2.5%

5.2. Radial position

The results for radial position were also presented in **Figure 3**. Here the data points represent the algorithm predictions for each of the 36 test points for all 3 damage sizes. The y-axis limits represent ±4% error bounds (relative to 25 cm). A summary of the absolute value and percentage of maximum and average error can be seen in **Table 2**. Overall, the average error for all cases was 2.4 mm (0.9%), with no apparent angular dependency, as anticipated by inspecting equation (8). No damage size dependency on error was apparent in the absolute sense, however an interesting trend observed was that as damage size increased, the algorithm tended to under-predict the distance to damage more frequently. This seems intuitive, since the damage boundaries are physically moving closer to the SHM node, however it is not straightforward enough of a relationship to compensate for in the algorithm.

Table 2: Maximum and average radial position prediction error

Damage (mm)	*Max. Error (mm)*	*Max. Error (%)*	*Avg. Error (mm)*	*Avg. Error (%)*
3.18	6.2	2.5%	3.2	1.3%
6.35	4.3	1.7%	1.1	0.4%
12.7	6.5	2.6%	2.8	1.1%

6. CONCLUSIONS

This paper presents proof-of-concept results for a patent-pending co-located triangulation methodology. A novel SHM node design and an innovative damage location algorithm were developed. A prototype system was applied to a large aluminum plate to demonstrate the technology. While not achieving theoretical accuracy levels, the overall results from proof-of-concept experiments were very impressive. Through a full range of angles around a 0.5 meter diameter circle, the average angular prediction error was <2.5% and the average radial prediction error was <1.0% for 3 sizes of representative damage (3.18, 6.35 and 12.7 mm diameter). Reconciling these averages, using this methodology a single 25 mm diameter SHM node could locate damage as small as 8 mm^2 anywhere within a 0.5 m diameter circle (1963.5 cm^2) to within an area of uncertainty of <1.0 cm^2. This result would provide more than sufficient information for an operator to make an informed maintenance decision, particularly if this method was combined with an algorithm that can determine damage type and severity as previously published by the present investigators [10]. Future work will aim to integrate these algorithms, as well as to improve accuracy through enhanced peak detection routines and implementing the described higher-speed miniature electronics. Overall, this methodology provides a path to reliable and efficient damage location detection while minimizing sensor density.

7. REFERENCES

[1] Lamb H. “On Waves in an Elastic Plate.” Proceedings of the Royal Society of London, Part A: Containing Papers of a Mathematical and Physical Character, v.93, n.651, 1917, 293-312.

[2] Kessler S.S., Spearing S.M. and C. Soutis. “Structural Health Monitoring in Composite Materials using Lamb Wave Methods.” *Smart Materials and Structures*, v.11, April 2002, 269-278.

[3] Olson S.E., DeSimio M.P. and M.M. Derriso. “Analytical Modeling of Lamb Waves for Structural Health Monitoring” AFRL report AFRL-VA-WP-TP-2006-320, March 2006.

[4] Dalton R.P., Cawley P. and M.J.S. Lowe. “The Potential of Guided Waves for Monitoring Large Areas of Metallic Aircraft Fuselage Structure.” Journal of NDE, v.20, 2001, 29-46.

[5] Raghavan A. and C.E.S. Cesnik. “Review of Guided-Wave SHM,” *The Shock and Vibration Digest*, v. 39, p. 91-114, 2007

[6] Derriso M. M., Olson S. E., Desimio M. P. And D. M. Pratt. “Why Are There Few Fielded SHM Systems for Aerospace Structures?” Proceedings of the 6th International Workshop on SHM, 11-14 September 2007, Stanford University.

[7] Kessler S.S. "Piezoelectric-Based In-Situ Damage Detection of Composite Materials for SHM Systems." Massachusetts Institute of Technology, Ph.D. Thesis, January 2002.

[8] Kessler S.S. and D.J. Shim."Validation of a Lamb Wave-Based SHM System for Aircraft Applications." Proceedings of the SPIE's 12th International Symposium on Smart Structures and Materials, 7-10 March 2005, San Diego, CA.

[9] Raghavan A. and C.E.S. Cesnik. “Finite Dimensional Piezoelectric Transducer Modeling for Guided Wave based SHM,” *Smart Materials and Structures*, v. 14, p. 1448-1461, 2005.

[10] Kessler S.S. and P. Agrawal. "Application of Pattern Recognition for Damage Classification in Composite Laminates." Proceedings of the 6th International Workshop on SHM, 11-14 September 2007, Stanford University.